Li_7GeS_5Br—An Argyrodite Li-Ion Conductor Prepared by Mechanochemical Synthesis

Florian Strauss, Tatiana Zinkevich, Sylvio Indris, Torsten Brezesinski

Abstract

In recent years, the search for glassy and ceramic Li^+ superionic conductors is receiving significant attention, mainly due to the renaissance of interest in all-solid-state batteries. Here, we report the mechanochemical synthesis of metastable Li_7GeS_5Br, which is, to the best of our knowledge, the first compound of the Li_2S-GeS_2-LiBr system. Applying combined synchrotron X-ray diffraction and neutron powder diffraction, we show Li_7GeS_5Br to crystallize in the *F*−43*m* space group and to be isostructural to argyrodite-type Li_6PS_5Br, but with a distinct difference in the S^{2-}/Br^- site disorder (and improved anodic stability). Electrochemical impedance spectroscopy indicates an electrical (ionic) conductivity of 0.63 mS cm^{-1} at 298 K, with an activation energy for conduction of 0.43 eV. This is supported by temperature-dependent ^7Li pulsed-field gradient-nuclear magnetic resonance spectroscopy measurements. Taken together, the results demonstrate that novel (metastable) argyrodite-type solid electrolytes can be prepared via mechanochemistry that are not accessible by conventional solid-state synthesis routes.

Introduction

State-of-the-art Li-ion batteries relying on the use of liquid carbonate-based electrolytes play an important role both in powering portable electronics and in electrifying transportation.[1] However, they are clearly about to approach their physicochemical limits in terms of energy density while the demand for improved energy storage technologies is ever increasing, especially to enable long-range electric vehicles.[2,3] In addition, liquid organic electrolytes are known to cause safety problems under harsh operating conditions and exhibit performance limitations, primarily at low and high temperatures. Substitution of the liquid electrolyte by a superionic solid inorganic electrolyte offers an interesting option to overcome such issues.[4,5] Some suitable materials have been reported in the past years, with sulfide-based Li-ion conductors emerging as one of the most promising because of their mechanical softness, among others. Note that the latter allows for high ionic conductivity even when cold pressing is used.[6–8] Nevertheless, the quest for novel Li^+ superionic ceramics, glasses, and glass-ceramics is ongoing.

Argyrodite-type solid electrolytes, represented by Li_6PS_5X (with X = Cl^-, Br^-, I^-), have early been recognized to possess fast Li mobility.[9,10] In recent years, large efforts have been made to further improve their charge transport properties (ion dynamics). In fact, the ionic conductivity has been increased successfully by anion and/or cation doping or substitution (i.e., replacing P^{5+} or S^{2-} with other elements).[11–15] In particular, Si^{4+}, Ge^{4+}, and Sn^{4+} have been substituted for P^{5+} in Li_6PS_5X, leading to compositions of the type $Li_{6+x}M_xP_{1-x}S_5X$; however, full substitution has not been achieved yet.[16–18] In these studies, high-temperature solid-state synthesis was chosen as the preferred preparation route, making the identification of metastable and low-temperature phases difficult or even impossible (despite the fact that Li_6PS_5X solid electrolytes can be prepared mechanochemically).[19–22]

Having this in mind, in the present work, we aimed at the possibility of substituting Ge^{4+} for P^{5+} in Li_6PS_5Br. Specifically, we report the successful synthesis of metastable Li_7GeS_5Br and demonstrate, by synchrotron X-ray diffraction (XRD) and neutron powder diffraction (NPD) combined with Rietveld refinement analysis, that this material is isostructural to related Li_6PS_5X argyrodites, but possesses a larger degree of S^{2-}/Br^- site disorder than Li_6PS_5Br. The ionic conductivity determined by temperature-dependent electrochemical impedance spectroscopy (EIS) and ^7Li pulsed-field gradient-nuclear magnetic resonance (^7Li PFG-NMR) spectroscopy was in the range between 0.78 and 0.82 mS cm^{-1} at 303 K. In addition, linear sweep voltammetry (LSV) indicated that the Li_7GeS_5Br has high anodic stability. Overall, these results are promising and emphasize the potential that mechanochemistry has in preparing novel Li^+ superionic conductors for application in practical all-solid-state batteries.[21,23–28]

Experimental Section

Synthesis

GeS_2 was prepared by mixing GeS (99.99%; Sigma-Aldrich) and S_8 (99.98%; Sigma-Aldrich) in a 70 mL zirconia jar with ten 10 mm diameter zirconia balls for 12 h at 250

rpm (with 1 h rest period after 6 h) using a planetary ball-mill (Fritsch). The total amount of powder was ~2.6 g, and sulfur was used in excess by 6 mol%. Subsequently, ~600 mg of mixture were pressed into a 10 mm diameter pellet at 1.5 t and sealed under vacuum ($1.0 \cdot 10^{-3}$ mbar) in a quartz ampoule. Note that the quartz ampoule was pre-dried for at least 15 min at 650 °C under dynamic vacuum using a heat-gun. The loaded ampoule was then heated to 450 °C at a slow rate of 27.5 °C h^{-1} to avoid bursting because of excessive sulfur evaporation, followed by annealing for 24 h.

Li_7GeS_5Br was prepared by milling stoichiometric amounts of GeS_2, LiBr (99.99%; Sigma-Aldrich), and Li_2S (99.99%; Sigma-Aldrich) in a 70 mL zirconia jar with twenty 10 mm diameter zirconia balls for 1 h at 250 rpm. The total amount of powder was ~1.1 g. The rotating speed was then increased to 450 rpm, and the milling was continued for 10 h without intermediate cooling.

In order to study the effect of annealing on the phase composition, ~150 mg of Li_7GeS_5Br were pressed into a 10 mm diameter pellet at 1.5 t, vacuum sealed in a quartz ampoule, and heated at 5 °C min^{-1} to the desired temperature (with 12 h dwell time) using a box furnace (Nabertherm).

Characterization

Laboratory XRD was conducted on a STADI P diffractometer (STOE) equipped with a Cu-$K\alpha_1$ radiation source (λ = 1.54056 Å). Samples were flame-sealed in borosilicate glass capillaries (Hilgenberg) of inner diameter 0.48 mm and wall thickness 0.01 mm.

Synchrotron XRD patterns were recorded in transmission geometry (λ = 0.412703 Å) at the 11-BM beamline of Argonne National Laboratory. Samples were mixed using mortar and pestle with 40 wt.% Si (99.998%; Sigma-Aldrich) under argon atmosphere and flame-sealed in borosilicate glass capillaries, which were then inserted into the Kapton tube of the sample holder.

NPD data were collected using the high-resolution powder diffractometer SPODI at MLZ in Garching (λ = 1.5482 Å). Samples were sealed under argon in vanadium containers.

Rietveld analysis of XRD and NPD patterns was done using FullProf software. The Thompson-Cox-Hastings pseudo-Voigt function was used to describe the profile (shape) of the reflections. Scale factor, background coefficients using a Chebyshev function with 24 parameters, reflection shape parameters, lattice parameters, atomic coordinates (except Li1 and Li2 [XRD] as well as S2 [NPD]), S^{2-}/Br^- site disorder, and zero-shift were refined. Note that S2 in the NPD refinement was fixed to avoid divergence. Isotropic displacement factors were fixed in both refinement analyses.

Differential scanning calorimetry (DSC) measurements were performed at a heating rate of 5 °C min^{-1} on a NETZSCH DSC 204 F1 Phoenix. Samples were sealed in aluminum crucibles under argon atmosphere.

The ionic conductivity was measured by EIS from 25 to 65 °C in the frequency range 100 mHz to 7.0 MHz with an AC voltage amplitude of 30 mV using an SP-300 potentiostat (Biologic). ~180 mg of Li_7GeS_5Br were compressed for 3.5 min at 3 t using a custom cell setup with stainless steel electrodes. A pressure of 40 MPa was maintained during the measurement. Impedance spectra were fitted with an $(R_1Q_1)Q_2$

equivalent circuit. The conductivity was calculated from the value of R_1, and the activation energy was determined by linear fitting of the temperature-dependent conductivity using the Arrhenius equation. Residual porosity was not taken into account, thus underestimated conductivity values may be assumed.

The electronic partial conductivity was determined by DC polarization at 25 °C and with DC voltages ranging from 0.2 to 1.0 V. The experiments were performed using a similar setup as for the EIS measurements. The resistance and conductivity were calculated from the steady-state current.

The anodic and cathodic stability of Li_7GeS_5Br was determined by LSV at 25 °C in the voltage range between 0 and 5 V vs Li^+/Li in a two-electrode cell with lithium metal as counter- and reference electrode and stainless steel as working electrode using a VMP3 potentiostat (Biologic). The sweep rate was 0.05 mV s^{-1}. ~100 mg of Li_7GeS_5Br were compressed for 3.5 min at 3 t using a custom cell setup and then contacted on one side by stainless steel and on the other side by a lithium metal disc (9 mm diameter; Albemarle Corp.). A pressure of 40 MPa was maintained during the measurement.

^{6}Li magic-angle spinning (^{6}Li MAS) NMR spectroscopy was performed on a Bruker Avance 500 MHz spectrometer at a magnetic field of 11.7 T, corresponding to a resonance frequency of 73.6 MHz. Spectra were acquired with a single pulse sequence, $\pi/2$ pulse length of 2.8 μs, and recycle delay of 30 s, and are referenced to an aqueous 1 M ^{6}LiCl solution at 0 ppm. Spinning was done in 2.5 mm rotors at 30 kHz.

^{7}Li PFG-NMR spectroscopy was performed on a Bruker Avance 300 MHz spectrometer equipped with a PFG-NMR probe, providing pulsed-field gradients up to 30 T m^{-1}. A stimulated-echo pulse sequence was applied with bipolar gradients, gradient duration of 2.75 ms, and diffusion time of 100 ms. The activation energy was determined by linear fitting of the temperature-dependent diffusion data using the Arrhenius equation. The ionic conductivity was calculated from the diffusion coefficient using the Nernst-Einstein equation.

Results and Discussion

The synthesis of Li_7GeS_5Br was attempted via mechanochemistry. Specifically, stoichiometric mixtures of Li_2S, GeS_2 (prepared from GeS and S_8; see XRD pattern and Le Bail fit in Figure S1 of the Supporting Information), and LiBr were subjected to high-energy ball-milling while monitoring the structural changes *ex situ* by XRD. Bragg reflections of both Li_2S and LiBr, along with minor ones corresponding to Li_7GeS_5Br, were observed after 5 h of milling (Figure 1a). Upon increasing the milling time to 8 h, the reflections of the newly formed phase became the major ones, and after 10 h, only those of Li_7GeS_5Br were evident in the pattern. Nevertheless, the reflection broadening and pattern background suggest a crystallite size in the nanometer size regime and the presence of amorphous side products or impurities.

In order to examine whether the crystallinity of Li_7GeS_5Br can be improved by post annealing, DSC was conducted on the sample milled for 10 h (Figure 1b). Exothermic

peaks were clearly visible at 258 (strong) and 314 °C (weak). Subsequently, the Li_7GeS_5Br sample was heated in quartz ampoules at 250 and 450 °C and then probed using XRD (Figure 1c). Annealing at 250 °C was already found to be accompanied by decomposition of the starting material. Bragg reflections associated with LiBr and Li_4GeS_4 appeared in the pattern, which further increased in intensity and decreased in broadening with annealing at 450 °C. This result thus suggests that the mechanochemically prepared Li_7GeS_5Br phase is metastable, in agreement with literature reports where substitution limits have been observed for related $Li_{6+x}M_xP_{1-x}S_5X$ (with M = Si^{4+}, Ge^{4+}, Sn^{4+} and X = Br^-, I^-) compounds produced by high-temperature solid-state synthesis.[16–18]

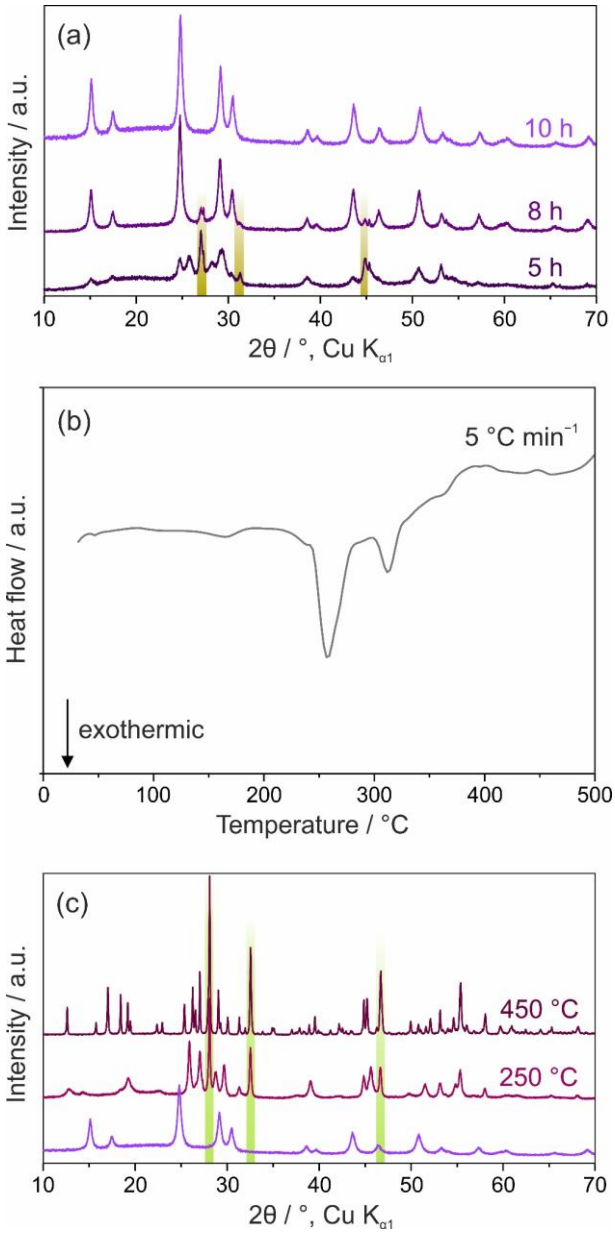

Figure 1. (a) XRD patterns of the precursor mixture after ball-milling for 5, 8, and 10 h. Reflections of Li_2S are highlighted for clarity. (b) DSC curve for Li_7GeS_5Br (after 10 h of milling) and (c) XRD patterns before and after annealing at 250 and 450 °C. Reflections of LiBr are highlighted for clarity.

In order to gain more structural insights, first synchrotron XRD data were collected for the Li_7GeS_5Br sample milled for 10 h. The experimental pattern can be indexed to the *F*−43*m* space group, based on a structure model reported for related argyrodite-type Li-ion conductors (Li_6PS_5Br),[29] with lattice parameter *a* = 10.18179(7) Å and ~60% S^{2-}/Br^- site disorder (Figure 2a). Note that the Li atomic coordinates were fixed in the Rietveld refinement, due to the low X-ray scattering form factor of lithium. Structural parameters and figure of merits are provided in Table S1 of the Supporting Information. Moreover, the fraction of amorphous side products was estimated at ~13 wt.%.

NPD was also performed to probe the Li substructure. A Rietveld plot for the refinement is shown in Figure 2b. In that case, the Li atomic coordinates were refined, and the *a* lattice parameter was found to be 10.17937(2) Å (details in Table S2 of the Supporting Information). Taken together, the incorporation of Ge^{4+} (i.e., $Li_{6+x}Ge_xP_{1-x}S_5Br$ with x = 1) led to an increase in lattice parameter by ~2%, which can be attributed to the larger ionic radius of Ge^{4+} than P^{5+}.[9]

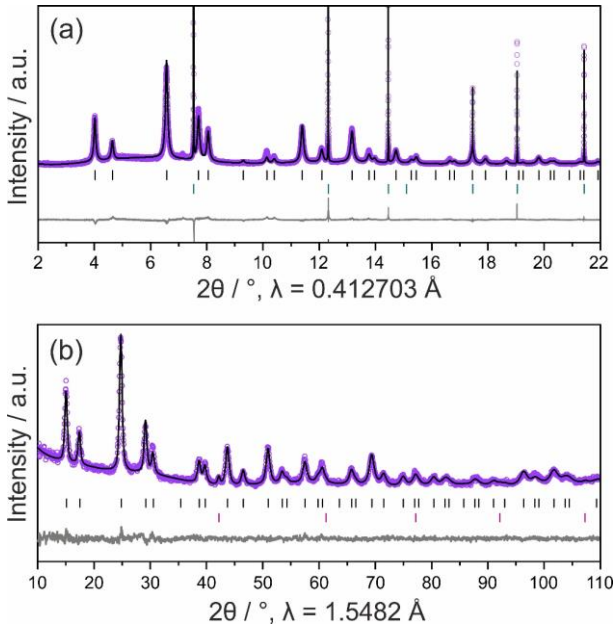

Figure 2. (a) Synchrotron XRD pattern of Li_7GeS_5Br mixed with 40 wt.% Si standard. Purple circles and black and gray lines represent the measured, calculated, and difference patterns, respectively. Black and cyan vertical lines (tick marks) denote the reflections for Li_7GeS_5Br and Si, respectively. The minor reflection around 7° 2θ is due to an unknown impurity. (b) NPD pattern of Li_7GeS_5Br, with purple circles and black and gray lines showing the measured, calculated, and difference patterns, respectively. Black and pink vertical lines (tick marks) denote the reflections for Li_7GeS_5Br and V, respectively. See Tables S1 and S2 of the Supporting Information for structural parameters from the corresponding Rietveld refinement analysis.

The crystal structure of Li_7GeS_5Br is schematically shown in Figure 3a. It comprises $[GeS_4]^{4-}$ tetrahedra with (additional) isolated $S^{2-}$and Br^- distributed in the 4*a* and 4*d* Wyckoff positions. More specifically, the 4*a* and 4*d* sites are occupied by ~40 and 60% Br^-, respectively, leading to a formal S^{2-}/Br^- site disorder of ~60%. This is in clear contrast to the parent compound, Li_6PS_5Br, where only 14-20% site disorder have been

observed.[9,29] The Li ions are distributed over two partially occupied positions (48*h* and 24*g*) and form cage-like Frank-Kasper structures (polyhedra) around the 4*d* position (Figure 3b). Li−Li jump distances within and especially between the cages are known to have a strong effect on the ion transport. For Li_7GeS_5Br, intra-cage and inter-cage jump distances of 2.352 Å (48*h*−48*h*), 1.857 Å (48*h*−24*g*−48*h*), and 2.988 Å were found, in agreement with literature data for other argyrodite-type solid elelctrolytes.[9,16,17,29] We also note that ^{6}Li MAS NMR spectroscopy revealed a single resonance centered at 1.65 ppm (see Figure S2 of the Supporting Information), similar to recent findings for Li_6PS_5Br.[30] The sharp signal (~0.17 ppm FWHM) is indicative of fast Li-ion hopping and of no significant structural disorder in principle.

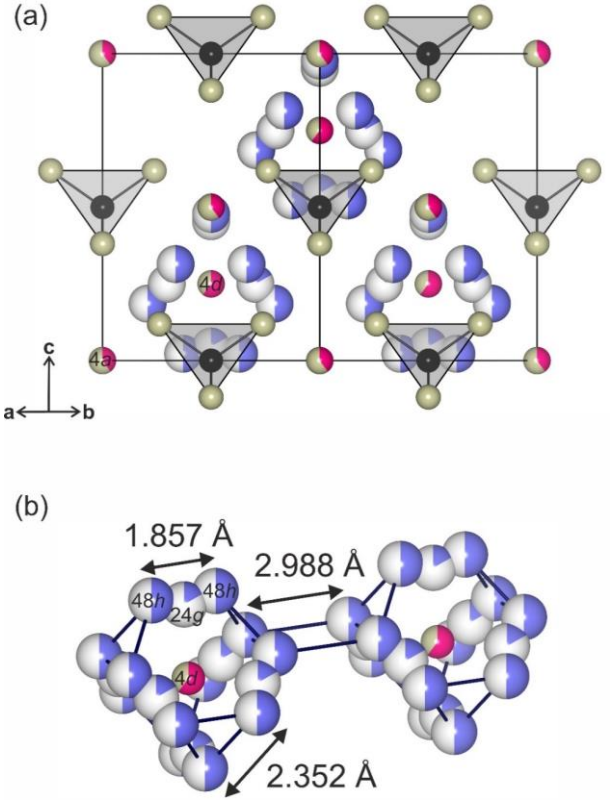

Figure 3. (a) Schematic crystal structure of Li_7GeS_5Br. Lithium, germanium, sulfur, and bromine are in blue, black, gray, and pink, respectively. (b) Li^+ cages around the shared S^{2-}/Br^- 4*d* Wyckoff position. Li−Li jump distances are denoted.

Next, EIS measurements were conducted from 25 to 65 °C on cold-pressed pellets to characterize the electrical conductivity of Li_7GeS_5Br. The experimental spectra showed a partial (depressed) semicircle and a capacitive tail (see Figure 4a and Figure S3 of the Supporting Information). A capacitance of 0.7 pF for the semicircle was calculated, corresponding to the bulk response at high frequencies.[31] Using the temperature-dependent resistance from AC impedance spectroscopy, the conductivity and activation energy for conduction were determined. As shown in Figure 4b, the ionic conductivity increased linearly over the whole temperature range, with σ = 0.63 mS cm^{-1} at 298 K and E_A = 0.43 eV. We note that the ionic conductivity is probably affected to some extent by the presence of deleterious (amorphous) phases. The conductivity of related Li_6PS_5X (with X = Cl^-, Br^-) compounds has been shown to depend on the

degree of crystallinity, among others,[19,20] which can usually be tailored by treatment at elevated temperatures. Unfortunately, the metastability of Li_7GeS_5Br did not allow for such post annealing. The electronic conductivity was determined by the DC polarization technique to be $1.61 \cdot 10^{-9}$ S cm^{-1} at 25 °C (see Figure S4 of the Supporting Information), in agreement with recent findings for thiophosphate-based Li-ion conductors.[11,32]

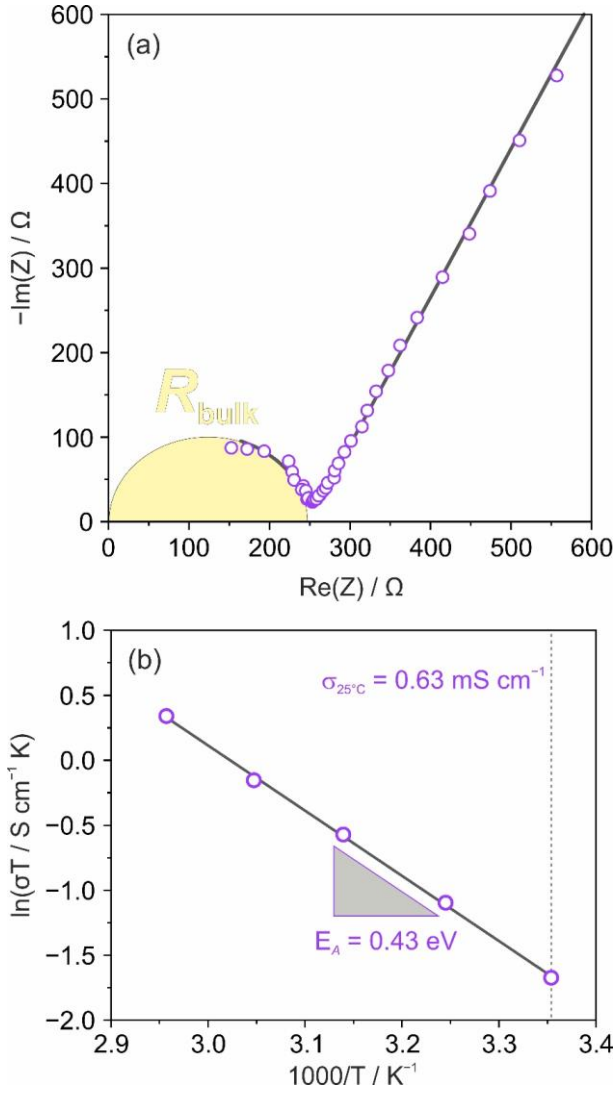

Figure 4. (a) Nyquist plot of the electrochemical impedance for Li_7GeS_5Br at 25 °C and the corresponding fitting to the experimental data. (b) Arrhenius fitting of the ionic conductivity in the temperature range between 25 and 65 °C.

Finally, ^{7}Li PFG-NMR spectroscopy measurements (probing the bulk) were performed in the temperature range between 30 and 60 °C to further examine the lithium diffusivity (see Figure S5 of the Supporting Information). Similar to what has been observed for lithium thiophosphates, Li_7GeS_5Br was found to exhibit a diffusion coefficient D = $4.8 \cdot 10^{-13}$ m^2 s^{-1} at 303 K.[11,33] The measured ^{7}Li diffusion coefficients are shown in Figure 5. From this data, an activation energy of 0.46 eV was determined, which is consistent with the results from EIS (Figure 4b). Using Nernst-Einstein equation, the ionic conductivity can be calculated from the diffusion coefficient (see Table S3 of the

Supporting Information). In so doing, for example, σ = 0.78 mS cm^{-1} at 303 K was obtained, which is also in good agreement with EIS for the same temperature (σ = 0.82 mS cm^{-1}). In addition, this result confirms our hypothesis that the electrical conductivity from EIS is somewhat affected by the presence of amorphous side products or impurities. Overall, the room-temperature ionic conductivity is comparable to that reported for other argyrodite-type solid electrolytes prepared mechanochemically (see Table S4 of the Supporting Information). Substituting Ge^{4+} for P^{5+} in Li_6PS_5Br apparently increased σ only slightly (0.63 vs 0.032-0.62 mS cm^{-1}),[10,19] thus emphasizing the complexity and difficulty to rationally designing novel Li^+ superionic conductors. However, it should be noted that several parameters have been reported to affect the charge transport properties (ion dynamics) to various degrees, site disorder being only one of them.

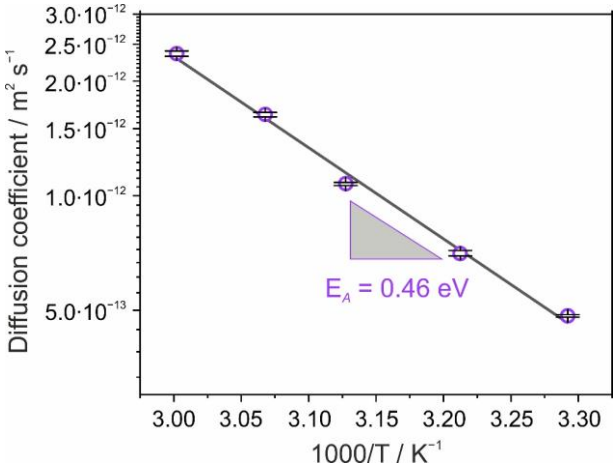

Figure 5. Temperature-dependent diffusion coefficient from ^{7}Li PFG-NMR spectroscopy. The solid line represents the Arrhenius fitting to the experimental data.

Yet another important characteristic of solid electrolytes, in particular for potential applications in all-solid-state batteries, is the electrochemical stability window. In order to assess the anodic and cathodic stability of Li_7GeS_5Br, LSV was performed at 25 °C and at a sweep rate of 0.05 mV s^{-1} using a two-electrode cell. The result of such measurement is shown in Figure S6 of the Supporting Information. The material was found to be relatively stable up to ~5 V vs Li^+/Li (no current onset was seen). In contrast, the cathodic stability was poor, especially below 1 V vs Li^+/Li, where distinct degradation of Li_7GeS_5Br took place, probably associated with the reduction of Ge^{4+}, as has been shown for other Ge-based solid electrolytes, such as $Li_{10}GeP_2S_{12}$.[34]

Conclusion

In summary, we have successfully prepared nanocrystalline (metastable) Li_7GeS_5Br by facile mechanochemical synthesis. Using synchrotron X-ray and neutron diffraction, Li_7GeS_5Br was found to crystallize in the *F*−43*m* space group and to adopt the argyrodite structure with tetrahedral $[GeS_4]^{4-}$ units and shared S^{2-}/Br^- sites (4*a* and 4*d* Wyckoff positions) with ~60% site disorder, compared to 14-20% for argyrodite-type Li_6PS_5Br. AC electrochemical impedance spectroscopy revealed a room-temperature

ionic conductivity of 0.63 mS cm^{-1} and an activation energy for conduction of 0.43 eV. ^{7}Li pulsed-field gradient-nuclear magnetic resonance spectroscopy measurements support these results. Because of the relatively low crystallinity and presence of impurities (amorphous side products), there is clearly room for further enhancements. Overall, our experimental data are promising and call for future investigations into substitution of P^{5+} by Si^{4+}, Ge^{4+}, and Sn^{4+} in related Li_6PS_5X (with X = Cl^-, Br^-, I^-) solid electrolytes using mechanochemical methods.

Associated Content

Supporting information

The Supporting Information is available free of charge on the ACS Publications website at DOI:

Le Bail fit of the XRD pattern for GeS_2. ^{6}Li MAS NMR spectrum and temperature-dependent Nyquist plots of the electrochemical impedance for Li_7GeS_5Br. Results from DC polarization experiments and ^{7}Li PFG-NMR spectroscopy. Electrochemical stability window of Li_7GeS_5Br from LSV. Structural parameters for Li_7GeS_5Br from XRD and NPD. Temperature-dependent diffusion coefficient from ^{7}Li PFG-NMR spectroscopy and calculated ionic conductivity. Room-temperature ionic conductivity of various mechanochemically prepared argyrodite-type solid electrolytes.

Author information

Corresponding author

Florian Strauss — *Battery and Electrochemistry Laboratory (BELLA), Institute of Nanotechnology, Karlsruhe Institute of Technology (KIT), Hermann-von-Helmholtz-Platz 1, 76344 Eggenstein-Leopoldshafen, Germany;* Email: florian.strauss@kit.edu

Authors

Tatiana Zinkevich — *Institute for Applied Materials−Energy Storage Systems (IAM-ESS), Karlsruhe Institute of Technology (KIT), Hermann-von-Helmholtz-Platz 1, 76344 Eggenstein-Leopoldshafen, Germany; Helmholtz Institute Ulm (HIU) Electrochemical Energy Storage, 89081 Ulm, Germany*

Sylvio Indris — *Institute for Applied Materials−Energy Storage Systems (IAM-ESS), Karlsruhe Institute of Technology (KIT), Hermann-von-Helmholtz-Platz 1, 76344 Eggenstein-Leopoldshafen, Germany; Helmholtz Institute Ulm (HIU) Electrochemical Energy Storage, 89081 Ulm, Germany*

Torsten Brezesinski — *Battery and Electrochemistry Laboratory (BELLA), Institute of Nanotechnology, Karlsruhe Institute of Technology (KIT), Hermann-von-Helmholtz-Platz 1, 76344 Eggenstein-Leopoldshafen, Germany*

Complete contact information is available at: https://pubs.acs.org/

Notes

The authors declare no competing financial interest.

Acknowledgement

F.S. acknowledges the Fonds der Chemischen Industrie (FCI) for financial support through a Liebig fellowship. This study was partially supported by BASF SE. Use of the Advanced Photon Source at Argonne National Laboratory was supported by the U. S. Department of Energy, Office of Science, Office of Basic Energy Sciences, under Contract No. DE-AC02-06CH11357. The authors thank H. Geßwein and V. Baran for assistance in collecting the DSC and NPD data, respectively.

References

(1) Larcher, D.; Tarascon, J.-M. Towards Greener and More Sustainable Batteries for Electrical Energy Storage. *Nat. Chem.* **2015**, *7*, 19–29.

(2) Sun, Y.-K. High-Capacity Layered Cathodes for Next-Generation Electric Vehicles. *ACS Energy Lett.* **2019**, *4*, 1042–1044.

(3) Erickson, E. M.; Ghanty, C.; Aurbach, D. New Horizons for Conventional Lithium Ion Battery Technology. *J. Phys. Chem. Lett.* **2014**, *5*, 3313–3324.

(4) Janek, J.; Zeier, W. G. A Solid Future for Battery Development. *Nat. Energy* **2016**, *1*, 16141.

(5) Robinson, A. L.; Janek, J. Solid-State Batteries Enter EV Fray. *Mrs Bull.* **2014**, *39*, 1046–1047.

(6) Lau, J.; DeBlock, R. H.; Butts, D. M.; Ashby, D. S.; Choi, C. S.; Dunn, B. S. Sulfide Solid Electrolytes for Lithium Battery Applications. *Adv. Energy Mater.* **2018**, *8*, 1800933.

(7) Lee, H.; Oh, P.; Kim, J.; Cha, H.; Chae, S.; Lee, S.; Cho, J. Advances and Prospects of Sulfide All-Solid-State Lithium Batteries via One-to-One Comparison with Conventional Liquid Lithium Ion Batteries. *Adv. Mater.* **2019**, *31*, 1900376.

(8) Zhang, Z.; Shao, Y.; Lotsch, B.; Hu, Y.-S.; Li, H.; Janek, J.; Nazar, L. F.; Nan, C.-W.; Maier, J.; Armand, M.; Chen. L. New Horizons for Inorganic Solid State Ion Conductors. *Energy Environ. Sci.* **2018**, *11*, 1945–1976.

(9) Deiseroth, H.-J.; Kong, S.-T.; Eckert, H.; Vannahme, J.; Reiner, C.; Zaiß, T.; Schlosser, M. Li_6PS_5X: A Class of Crystalline Li-Rich Solids With an Unusually High Li^+ Mobility. *Angew. Chem. Int. Ed.* **2008**, *47*, 755–758.

(10) Rao, R. P.; Adams, S. Studies of Lithium Argyrodite Solid Electrolytes for All-Solid-State Batteries. *Phys. Status Solidi A* **2011**, *208*, 1804–1807.

(11) Adeli, P.; Bazak, J. D.; Park, K. H.; Kochetkov, I.; Huq, A.; Goward, G. R.; Nazar, L. F. Boosting Solid-State Diffusivity and Conductivity in Lithium Superionic Argyrodites by Halide Substitution. *Angew. Chem. Int. Ed.* **2019**, *58*, 8681–8686.

(12) Zhou, L.; Assoud, A.; Zhang, Q.; Wu, X.; Nazar, L. F. New Family of Argyrodite Thioantimonate Lithium Superionic Conductors. *J. Am. Chem. Soc.* **2019**, *141*, 19002–19013.

(13) Bernges, T.; Culver, S. P.; Minafra, N.; Koerver, R.; Zeier, W. G. Competing Structural Influences in the Li Superionic Conducting Argyrodites $Li_6PS_{5-x}Se_xBr$ ($0 \leq x \leq 1$) upon Se Substitution. *Inorg. Chem.* **2018**, *57*, 13920–13928.

(14) Schlem, R.; Ghidiu, M.; Culver, S. P.; Hansen, A.-L.; Zeier, W. G. Changing the Static and Dynamic Lattice Effects for the Improvement of the Ionic Transport Properties within the Argyrodite $Li_6PS_{5-x}Se_xI$. *ACS Appl. Energy Mater.* **2020,** *3*, 9–18.

(15) de Klerk, N. J. J.; Rosłoń, I.; Wagemaker, M. Diffusion Mechanism of Li Argyrodite Solid Electrolytes for Li-Ion Batteries and Prediction of Optimized Halogen Doping: The Effect of Li Vacancies, Halogens, and Halogen Disorder. *Chem. Mater.* **2016**, *28*, 7955–7963.

(16) Ohno, S.; Helm, B.; Fuchs, T.; Dewald, G.; Kraft, M. A.; Culver, S. P.; Senyshyn, A.; Zeier, W. G. Further Evidence for Energy Landscape Flattening in the Superionic Argyrodites $Li_{6+x}P_{1-x}M_xS_5I$ (M = Si, Ge, Sn). *Chem. Mater.* **2019**, *31*, 4936–4944.

(17) Minafra, N.; Culver, S. P.; Krauskopf, T.; Senyshyn, A.; Zeier, W. G. Effect of Si Substitution on the Structural and Transport Properties of Superionic Li-Argyrodites. *J. Mater. Chem. A* **2018**, *6*, 645–651.

(18) Zhao, F.; Liang, J.; Yu, C.; Sun, Q.; Li, X.; Adair, K.; Wang, C.; Zhao, Y.; Zhang, S.; Li, W.; Deng, S.; Li, R.; Huang, Y.; Huang, H.; Zhang, L.; Zhao, S.; Lu, S.; Sun, X. A Versatile Sn-Substituted Argyrodite Sulfide Electrolyte for All-Solid-State Li Metal Batteries. *Adv. Energy Mater.* **2020**, *10*, 1903422.

(19) Boulineau, S.; Courty, M.; Tarascon, J.-M.; Viallet, V. Mechanochemical Synthesis of Li-Argyrodite Li_6PS_5X (X = Cl, Br, I) as Sulfur-Based Solid Electrolytes for All Solid State Batteries Application. *Solid State Ionics* **2012**, *221*, 1–5.

(20) Yu, C.; Ganapathy, S.; Hageman, J.; van Eijck, L.; van Eck, E. R. H.; Zhang, L.; Schwietert, T.; Basak, S.; Kelder, E. M.; Wagemaker, M. Facile Synthesis toward the Optimal Structure-Conductivity Characteristics of the Argyrodite Li_6PS_5Cl Solid-State Electrolyte. *ACS Appl. Mater. Interfaces* **2018**, *10*, 33296–33306.

(21) Boulineau, S.; Tarascon, J.-M.; Leriche, J.-B.; Viallet, V. Electrochemical Properties of All-Solid-State Lithium Secondary Batteries Using Li-Argyrodite Li_6PS_5Cl as Solid Electrolyte. *Solid State Ionics* **2013**, *242*, 45–48.

(22) Rayavarapu, P. R.; Sharma, N.; Peterson, V. K.; Adams, S. Variation in Structure and Li^+-Ion Migration in Argyrodite-Type Li_6PS_5X (X = Cl, Br, I) Solid Electrolytes. *J. Solid State Electrochem.* **2012**, *16*, 1807–1813.

(23) Machida, N.; Maeda, H.; Peng, H.; Shigematsu, T. All-Solid-State Lithium Battery with $LiCo_{0.3}Ni_{0.7}O_2$ Fine Powder as Cathode Materials with an Amorphous Sulfide Electrolyte. *J. Electrochem. Soc.* **2002**, *149*, A688–A693.

(24) Hayashi, A.; Konishi, T.; Tadanaga, K.; Minami, T.; Tatsumisago, M. All-Solid-State Lithium Secondary Battery with SnS–P_2S_5 Negative Electrodes and Li_2S–P_2S_5 Solid Electrolytes. *J. Power Sources* **2005**, *146*, 496–500.

(25) Minami, T.; Hayashi, A.; Tatsumisago, M. Recent Progress of Glass and Glass-Ceramics as Solid Electrolytes for Lithium Secondary Batteries. *Solid State Ionics* **2006**, *177*, 2715–2720.

(26) Ulissi, U.; Agostini, M.; Ito, S.; Aihara, Y.; Hassoun, J. All Solid-State Battery Using Layered Oxide Cathode, Lithium-Carbon Composite Anode and Thio-LISICON Electrolyte. *Solid State Ionics* **2016**, *296*, 13–17.

(27) Strauss, F.; Bartsch, T.; de Biasi, L.; Kim, A-Y.; Janek, J.; Hartmann, P.; Brezesinski, T. Impact of Cathode Material Particle Size on the Capacity of Bulk-Type All-Solid-State Batteries. *ACS Energy Lett.* **2018**, *3*, 992–996.

(28) Bartsch, T.; Strauss, F.; Hatsukade, T.; Schiele, A.; Kim, A-Y.; Hartmann, P.; Janek, J.; Brezesinski, J. Gas Evolution in All-Solid-State Batteries. *ACS Energy Lett.* **2018**, *3*, 2539–2543.

(29) Kraft, M. A.; Culver, S. P.; Calderon, M.; Böcher, F.; Krauskopf, T.; Senyshyn, A.; Dietrich, C.; Zevalkink, A.; Janek, J.; Zeier, W. G. Influence of Lattice Polarizability on the Ionic Conductivity in the Lithium Superionic Argyrodites Li_6PS_5X (X = Cl, Br, I). *J. Am. Chem. Soc.* **2017**, *139*, 10909–10918.

(30) Hanghofer, I.; Brinek, M.; Eisbacher, S. L.; Bitschnau, B.; Volck, M.; Hennige, V.; Hanzu, I.; Rettenwander, D.; Wilkening, H. M. R. Substitutional Disorder: Structure and Ion Dynamics of the Argyrodites Li_6PS_5Cl, Li_6PS_5Br and Li_6PS_5I. *Phys. Chem. Chem. Phys.* **2019**, *21,* 8489–8507.

(31) Irvine, J. T. S.; Sinclair, D. C.; West, A. R. Electroceramics: Characterization by Impedance Spectroscopy. *Adv. Mater.* **1990**, *2,* 132–138.

(32) Sedlmaier, S. J.; Indris, S.; Dietrich, C.; Yavuz, M.; Dräger, C.; von Seggern, F.; Sommer, H.; Janek, J. Li_4PS_4I: A Li^+ Superionic Conductor Synthesized by a Solvent-Based Soft Chemistry Approach. *Chem. Mater.* **2017**, *29*, 1830–1835.

(33) Stöffler, H.; Zinkevich, T.; Yavuz, M.; Hansen, A.-L.; Knapp, M.; Bednarčík, J.; Randau, S.; Richter, F. H.; Janek, J.; Ehrenberg, H.; Indris, S. Amorphous versus Crystalline Li_3PS_4: Local Structural Changes during Synthesis and Li Ion Mobility. *J. Phys. Chem. C* **2019**, *123*, 10280–10290.

(34) Wenzel, S.; Randau, S.; Leichtweiß, T.; Weber, D. A.; Sann, J.; Zeier, W. G.; Janek, J. Direct Observation of the Interfacial Instability of the Fast Ionic Conductor $Li_{10}GeP_2S_{12}$ at the Lithium Metal Anode. *Chem. Mater.* **2016**, *28,* 2400–2407.

For Table of Contents Only

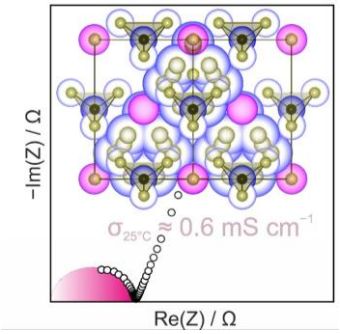

A novel argyrodite-type solid electrolyte showing a room-temperature ionic conductivity of about 0.6 mS cm^{-1} has been prepared via mechanochemistry.